An Innovative Method for Predicting Parametric Dependent-Pressure Drops of Meandering Magnetorheological Valves Using Deep Neural Networks

Hafizh Arsa Prabhakara[1], Fitrian Imaduddin[2,3], Azizan As'arry[4], Andhi Akhmad Ismail[1], Saiful Amri Mazlan[5], Irfan Bahiuddin[1*]

[1] Department of Mechanical Engineering, Vocational College, Universitas Gadjah Mada, Yogyakarta, Indonesia
[2] Mechanical Engineering Department, Faculty of Engineering, Islamic University of Madinah, Medina, Saudi Arabia
[3] Mechanical Engineering Department, Faculty of Engineering, Universitas Sebelas Maret, Surakarta, Indonesia
[4] Department of Mechanical and Manufacturing Engineering, Faculty of Engineering, Universiti Putra Malaysia, Serdang, Selangor, Malaysia
[5] Malaysia-Japan International Institute of Technology, Universiti Teknologi Malaysia Kuala Lumpur, Malaysia

Corresponding Author: irfan.bahiuddin @ugm.ac.id

Abstract

This paper introduces a novel approach for predicting magnetorheological (MR) valve pressure drop using deep neural networks. Rather than regressing the pressure drop directly, the proposed methodology predicts magnetic flux densities across different valve zones and then uses these predictions to compute the MR fluid's yield stress and the valve's pressure drop. The proposed approach can be further deployed for optimization purposes and provides insight into the magnetic field distribution within the MR valve as a function of design parameters. The approach leverages finite element simulations encompassing 125 variations of geometric parameters (gap sizes) and control parameters (electrical currents). A multilayer neural network architecture is tuned by testing 72 configurations of activation functions, numbers of hidden nodes, and layers, with model selection based on mean squared error and R^2. The final model demonstrates high fidelity with R^2 more than 0.98 for both training and testing. By capturing how magnetic flux density varies as a function of design and control parameters, the proposed framework facilitates efficient optimization and design of MR valves without exhaustive simulation. These results underscore the method's ability to capture the complex dynamics governing MR valve pressure drop and provide valuable insights for valve sizing and performance prediction.

Keywords: *design, deep neural networks, semi-active devices, magnetorheological valves, pressure drop, magnetorheological fluids*

1 Introduction

Magnetorheological (MR) fluids, serving as smart materials, exhibit controllable rheological properties when subjected to magnetic field stimuli. The evolution of these materials has matured with their widespread application in commercialized automotive MR dampers. It extends to diverse fields such as bridges [1], buildings [2], transportation [3], and medical devices [4], primarily in the form of MR dampers. The damper's main function lies in controlling energy dissipation, a task usually facilitated by the MR valve part [5]. This valve operates by creating obstructions and is controlled by exposure to magnetic fields. The conventional type of MR valve, allowing fluid to follow a simple path, has inherent limitations in controllability and damping force magnitude range. Consequently, various efforts have emerged to broaden the control range and achieve higher damping force magnitude.

Various methods have been proposed to address these challenges. One approach involves altering the fluid path, introducing turns and twists to fit compact spaces while generating higher drop pressure with limited space. The studies include a simple combination of the annular and radial paths [6]. A more complex pattern, namely the meandering flow path type, is proposed in the previous literature [7]. Further modification is conducted by Zhu et al. [8] by developing a multistage concept. Another effort focuses on enhancing magnetic flux density by employing a serpentine magnetic flux path. The magnetic field is driven to go through several turns while keeping a relatively high density, namely serpentine [9]. Disk and helix flow have recently been utilized to obtain more effective exposure to magnetic field density areas with relatively easier modification than the previous approaches [10]. However, these methods share a common trait—the need to tune complex parameters to obtain optimal valve performance. Traditional parameter tuning methods involve trial and error or systematic observation, which can be time-consuming. Meta-heuristic methods like genetic algorithms or particle swarm optimization offer automatic alternatives for parameter tuning [11]. The cost function needs to be carefully defined, consisting of models that can capture the correlation between the valve dimension and the pressure drop. Total pressure drop for MR devices is a combination of the drops at various paths affected directly by magnetic flux density distributions. Meanwhile, the distributions are affected by various aspects, such as the coil, materials, and valve dimension. Hence, the correlation between the valve dimension and pressure drop is highly nonlinear, as magnetic flux density is difficult to predict.

Several ways exist in the literature for predicting magnetic flux densities along the flow path as a function of parameters. The first method directly includes the magnetic simulation software in the optimization loop, providing a detailed but time-consuming process [12]. Another method is simple linear regression with ANOVA to check the influence [13]. The interpolation using response surface methodology or multilinear regression can also be conducted [14]. The limitations of the methods are the limited range and low accuracy

for complex correlations, such as including numerous design parameters [8] or the time response consideration [15]. The more advanced modeling methods, such as machine learning, can be alternative solutions. The method can be considered a physic-informed-machine learning approach by including the information on the design parameter or geometric information toward the model [16].

Machine learning approaches are available in the literature, including artificial neural networks (ANNs) [17], extreme learning machines (ELMs) [18], support vector regressions (SVRs) [19], and decision trees [20]. The models provide more accurate predictions and can accommodate more complex systems with more inputs. Various configurations are available depending on the complexity, from simple to deep neural networks (DNN). DNN has several advantages compared to classic machine learning methods, such as higher accuracy and the capability to learn complex behavior. Due to the advantages, the technique can be combined with various methods, such as reinforcement learning [21] and fuzzy logic algorithms [22]. It has been combined with multiple suspension models, including spring and hydraulic models, to predict the damper force [23]. In another damper device, Hu et al. [24] proposed a DNN application for predicting the hysteresis as a replacement for the Bouc-Wen model as a function of geometrical parameters. However, the existing works that employed DNN for predicting magnetic flux densities for an MR valve can be considered rare.

Therefore, this work proposed an approach to predict magnetic flux densities using DNN. The article encompasses a detailed methodology, data acquisition procedures, and descriptions of simulation results, comparing drop pressure and magnetic flux density with experimental and simulated data. Then, the performance of various machine learning methods is systematically compared and discussed.

2 Methodology

2.1 Proposed Platforms

Figure 1 outlines the sequential steps in building the proposed models, starting with the training process. In the training process, the model is utilized to predict magnetic flux densities, which are subsequently employed to forecast pressure drop using steady-state equations. Defining the input and output parameters of the deep learning-based feedforward neural networks requires a comprehensive understanding of the general structure of the MR valve. Deep learning, a subset of machine learning, utilizes artificial neural networks with multiple layers (deep architectures) to automatically extract features from input data, enabling highly accurate predictions. This study employs a relatively complex MR valve structure as a case study. This valve type with a meandering flow path has an advantage in compactness and peak drop pressure. Several parameters corresponding to the kind of paths need to be tuned, including the orifice, annular, and radial at the outer and inner part of the valve, as shown in Figure 2. Figure 3 provides an

overview of the input and output architecture of the proposed neural networks. Inputs include dimensions and electrical current, while outputs encompass magnetic flux densities across various regions. For predicting magnetic flux density, inputs are gap sizes and current.

The proposed methods can be deployed for optimization in the future. The optimization process is based on pressure drops and control ranges influenced by magnetic fields. Magnetic fields are influenced by the designs or topologies and given electrical currents to the coil. The design or topologies are mainly affected by the paths. The paths consist of radial, annular, and orifice paths. Radial and annular affect the pressure drops, while the orifice is not too significant, as discussed in the previous studies [25]. One of the design parameters is annular and radial gaps. The correlation between the minimum and maximum values of pressure drops and electrical currents affects the control ranges. In other words, the gaps represent the design parameters, while the electrical currents represent the controllability.

2.2 Machine Learning Methods

The artificial neural network modeling utilizes a feedforward neural network architecture and various hyperparameter configurations that can be observed in Table 1. Mean Squared Error (MSE) is chosen as the cost function as the parameter for determining the number of hidden layers and neurons [23]. Increasing the number of hidden layers can enhance the accuracy performance of the artificial neural network at a certain point. However, excessive hidden layers can make the network difficult to train, leading to potential overfitting [26]. Commonly used activation functions include ReLU, sigmoid, or tanh, with the typical range for the number of neurons in the hidden layer being 10 to 100. Adam's method is selected as the optimization algorithm for its adaptive learning rate capabilities and popularity in various optimization problems within neural networks [27]. The learning rate is a critical hyperparameter, typically adjusted to a value between 1 and 10^{-6} [28]. The batch size represents a fraction of the training data used to estimate the gradient during weight updates. A smaller batch size accelerates the training process, while a larger one provides a more accurate gradient estimate. This work utilizes 32 batch sizes. The selected variations for learning rate and batch size in this artificial neural network modeling range from 10^{-1} to 10^{-5} and from 1 to 32, respectively.

The dataset is divided into training, validation, and testing data sets with a 75%, 15%, and 15% ratio, respectively. The input data set, defined as x, undergoes normalization using Eq. (1). The normalized input, denoted as x_{norm}, is a function of the minimum value (x_{min}) and the maximum value (x_{max}) [29].

$$x_{norm} = \frac{x - x_{min}}{x_{max} - x_{min}} \quad (1)$$

The training process is conducted over 500 epochs. The accuracy of the modeling is measured using the R-squared (R^2), calculated according to Eq. (2). Here, y_e represents the target data, y_{mean} is the mean data, and y_p denotes the predicted data sequentially. K stands for the number of data sets [29].

$$R^2 = 1 - \frac{\sum_{h=1}^{K}(y_p - y_e)^2}{\sum_{h=1}^{K}(y_p - y_{mean})^2} \quad (2)$$

The method employed to determine the optimal hyperparameters for this artificial neural network is grid search cross-validation. Grid search is an approach to hyperparameter optimization that systematically builds and evaluates models for each predefined combination of hyperparameters in a grid. Meanwhile, cross-validation is used to resample data for evaluating machine learning models [30]. Figure 4 illustrates the grid search cross-validation process. Initially, the dataset is randomly divided and grouped according to fold parameters, where each fold serves as testing data, and the remaining folds constitute the training data. Evaluation scores are recorded for each split and averaged to review the performance of the artificial neural network modeling. This process is repeated until the n-th hyperparameter combination and the combination yielding the best performance is selected. In the grid search cross-validation for this artificial neural network modeling, the folds are divided into three parts, and the accuracy performance of the neural network is assessed based on the Mean Squared Error (MSE) values.

2.3 Data Preparation and Finite Element Method Magnetics

The training process, depicted in Figure 1, relies on Finite Element Methods Magnetics (FEMM) modeling validated against experimental data. The training phase of the artificial neural network employs multilayer feedforward neural networks, enhancing the model's ability to capture the intricate relationships within the meandering flow path-type MR valve. The meandering flow path-type MR valve structure consists of three main components: casing, coil, and valve core. The casing, made of AISI 1010, guides magnetic flux efficiently and secures the internal structure. The coil, composed of copper and aluminum windings, determines the magnetic field strength and acts as a flow channel wall. The valve core consists of side cores, orifice cores, a center core, and aluminum spacers. The entire valve has an outer diameter of 50 mm and an overall length of 77 mm.

The MR valve is divided into male and female casings, each made of AISI 1010 with threaded connections, and features female BSPP (British Standard Pipe Parallel) ¼ inch fluid ports. The coil consists of copper and aluminum windings with O-ring slots for sealing. The valve core, including side cores, orifice cores, a center core, and aluminum spacers, maintains clearances between components. The inner coil diameter is 15 mm. The annular and radial gaps and the channel length are varied to create a winding flow path. The casing thickness is 4 to 5 mm. Using 22 AWG copper wire, the coil has a total resistance of 2.23 Ω and is wound with 450 turns. A current limit of 1 A is applied to maintain a maximum power consumption of 2.23 W.

Numerical methods are employed to predict the magnetic circuit's performance in MR usage, evaluating magnetic field strength using finite element analysis with FEMM software. The MR valve's 2D axisymmetric projection is modeled, and material permeabilities are derived from B-H curves. The study incorporates the B-H curve of AISI 1010 for magnetic materials and aluminum for non-magnetic materials, as shown in Figure 5 [31]. The research presents the yield stress of MRF-132DG MR fluid from Lord Corporation graphically concerning magnetic flux density and yield stress.

As proposed by Nguyen et al. [32], a polynomial approach is employed to establish the yield stress equation ($\tau(B)$) using the B value, as shown in Eq. (3).

$$\tau(B) = 52.962B^4 + 176.51B^3 + 158.79B^2 + 13.708B + 0.1442 \quad (3)$$

From the equation, MRF-132DG reaches its saturation point at 1.2 T. The MR fluid's rheological properties are essential when determining the maximum current input for the coil in the meandering flow path-type MR valve design. Other crucial parameters include variables turn number and length of the coil.

Figure 6 illustrates the two-dimensional axisymmetric design of the meandering flow path-type MR valve in FEMM software. The design results include running mesh and analysis and providing graphical data and magnetic flux density files along the channel in the meandering flow path-type MR valve. After creating lines along the effective area, as shown in Figure 7, the magnetic flux density data is utilized as the artificial neural network modeling dataset. The observation line is always in the middle of the gap. For example, if the gap is 1.0, the observation line will be 0.5 from both nearest walls.

Figure 8 illustrates how the magnetic flux densities for training data are determined. The highest magnetic flux densities in annular, inner radial, and outer radial zones are treated as the training data. Meanwhile, the orifice and inner annular parts are assumed to be zero. The magnetic flux densities are considered to be symmetrical between the right and left parts of the MR valve. The assumption will be employed while calculating the pressure drops.

2.4 Pressure Drop Calculation

The pressure drop (ΔP) in the meandering flow path-type MR valve is divided into two components, which are viscous and yield pressure drops, as expressed in the quasi-steady Eq. (4). Eq. (5) illustrates that the viscous pressure drop for annular ($\Delta P_{viscous,annular}$) is related to the fluid's base viscosity (η), flow rate (Q), the annular valve channel's length (L), and inversely proportional to the channel radius (R). On the other hand, Eq. (6) shows that the yield pressure drop is associated with the yield stress ($\tau(B)$), L, and the flow velocity coefficient (c), inversely proportional to the gap size (d). c is calculated using Equation (7).

$$\Delta P = \Delta P_{viscous} + \Delta P_{yield} \tag{4}$$

$$\Delta P_{viscous,annular} = \frac{6\eta QL}{\pi d^3 R} \tag{5}$$

$$\Delta P_{yield,annular} = \frac{c\tau(B)L}{d} \tag{6}$$

$$c = 2.07 + \frac{12Q\eta}{12Q\eta + 0.8\pi R d^2 \tau(B)} \tag{7}$$

For MR valves with radial gaps, Eq. (8) and (9) describe viscous and yield pressure drops, respectively. R_0 and R_i refer to the outer and inner radial gaps, respectively. The proposed MR valve design incorporates both annular and radial gaps, resulting in combined mathematical equations. For orifice gaps, as magnetic flux is assumed to not pass through them, the pressure drop equation is based on the MR fluid's viscous properties, expressed by Eq. (10).

$$\Delta P_{viscous} = \frac{6\eta QL}{\pi d^3 R} \ln \frac{R_o}{R_i} \tag{8}$$

$$\Delta P_{yield} = \frac{c\tau\,(B)}{d}\,(R_o - R_i) \tag{9}$$

$$\Delta P = \frac{8\eta QL}{\pi R^4} \tag{10}$$

Different parts of the MR valve have distinct magnetic flux densities. Hence, the valve gaps are divided into five zones: outer annular gap, outer radial gap, inner annular gap, inner radial gap, and orifice gap. These zones are further categorized into effective area and viscous resistance. The effective area includes the outer annular, outer radial, and inner radial gaps, while the viscous resistance consists of the inner annular and orifice gaps. Eq. (11) shows the pressure drops at various zones, and each zone is defined by Eq. (12)-(16).

$$\Delta P_{valve} = \Delta P_{annular\_outer} + \Delta P_{radial\_outer} + \Delta P_{annular\_inner} + \Delta P_{radial\_inner} + \Delta P_{orifice} \tag{11}$$

$$\Delta P_{annular\_outer} = 2\left[\frac{6\eta Q L_{ao}}{\pi d_{ao}^3 R_{ao}} + \frac{c_a \tau_a(B) L_{ao}}{d_{ao}}\right] \quad (12)$$

$$\Delta P_{radial\_outer} = 2\left[\frac{6\eta Q}{\pi d_{ro}^3} ln\left(\frac{R_1}{R_{0\_outer}}\right) + \frac{c_a \tau_{ro}(B)}{d_{ro}}\left(R_1 - R_{0\_outer}\right)\right] \quad (13)$$

$$\Delta P_{annular\_inner} = 3\frac{6\eta Q L_{ai}}{\pi d_{ai}^3 R_{ai}} \quad (14)$$

$$\Delta P_{radial\_inner} = 4\left[\frac{6\eta Q}{\pi d_{ri}^3} ln\left(\frac{R_1}{R_{0\_inner}}\right) + \frac{c_{ri}\tau_{ri}(B)}{d_{ri}}\left(R_1 - R_{0\_inner}\right)\right] \quad (15)$$

$$\Delta P_{orifice} = 2\frac{8\eta Q L_o}{\pi R_{0\_inner}{}^4} \quad (16)$$

The MRF-132DG MR fluid used in this study is commercially available from Lord Corp. Key parameters for the meandering flow path-type MR valve are presented in Table 2.

The modeling with an artificial neural network aims to determine the magnetic flux density in the meandering flow path-type MR valve. The predicted values are then used in steady-state modeling to determine the pressure drop.

3 Results and Discussion

3.1 Hyper Parameter Variations

The study conducted a hyperparameter exploration to determine the optimal configuration for a neural network. The variations included the number of neurons in each hidden layer (ranging from 10 to 100), the number of hidden layers (1 to 3), and activation functions (Sigmoid, Tanh, and ReLU). The GridSearchCV Hyper parameter variations for machine learning are not too strict. For obtaining the best accuracy, different datasets can have different configurations. As for the proposed works, they can be considered new. Seventy-two configurations were tried, consisting of activation function variations, hidden node number variations, and layer number variations. Activation functions are sigmoid (sig), hyperbolic tangent (tanh), and rectifier linear units (ReLU). The hidden node numbers are small, medium, and large, consisting of 10, 50, and 100. Hidden node numbers in all hidden layers are the same. The process utilized the Adam optimization algorithm.

Table 3 shows the MSE at various activation functions and hidden node numbers. To simplify the problem, the hidden node number is assumed to be the same for all layers. Based on the table, ReLU activation with 100 neurons demonstrated the lowest mean squared error (MSE) of 0.07 for a single hidden layer. In the case of two hidden layers, the best configuration was 100 neurons in each layer, with ReLU activation in

both layers, resulting in an MSE of 0.06. Similarly, for three hidden layers, the optimal setup involved 100 neurons in each layer. ReLU activation in the first two layers and Tanh activation in the third, achieving an MSE of 0.06.

The findings indicate that the choice of the number of neurons in each hidden layer depends on the activation function and the number of hidden layers. Sigmoid activation was less suitable, consistently yielding higher MSE compared to the other two activation functions. The comparison of single, double, and triple hidden layer variations revealed that the architecture with three hidden layers performed the best, especially with 100 neurons in each layer containing ReLU, ReLU, and Tanh activations. From these three experiments with hidden layer variations, it can be concluded that the number of neurons in each hidden layer depends greatly on the activation function and the number of hidden layers to achieve the optimal number of neurons in each hidden layer. The sigmoid activation function appears less suitable for this artificial neural network modeling, as it consistently yields higher average MSE than the other two activation functions. Furthermore, variations with one, two, and three hidden layers are compared to determine the best artificial neural network model.

Further refinements involve tuning the learning rate and batch size, as shown in Figure 9. The exploration revealed that a learning rate of 10^{-3} and a batch size 16 resulted in the lowest MSE of 0.06, indicating optimal model accuracy and mitigating the risk of overfitting. The selection of an appropriate learning rate is paramount, as an excessively high value can engender training divergence, whereas an exceedingly low value prolongs the training process. Thus, carefully selecting the learning rate enhanced the accuracy of the artificial neural network model.

The training results, represented by MSE values, are provided for different zones (annular outer, radial outer, and radial inner), as shown in Figure 10

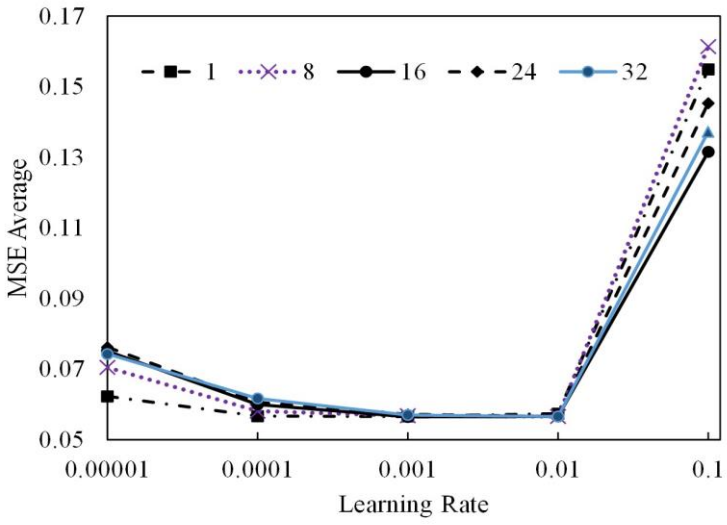

Figure 9. MSE at various learning rates and batch sizes

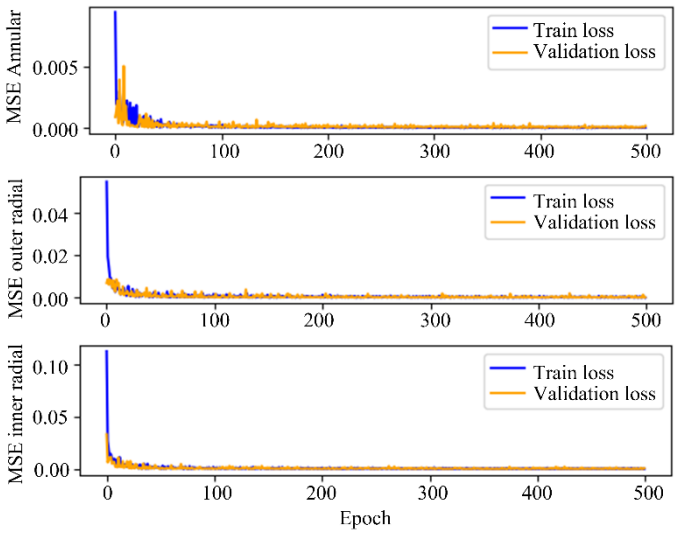

Figure 10. The trained model generally accurately predicts magnetic flux densities in various zones. The MSE reaches steady values at less than 100 epochs. Therefore, for the next training process, an early stop at an epoch of 100 can be applied to prevent training that is too long or hyperparameter tuning times. Furthermore, the optimization method to predict the best hyperparameter can be used at iteration less than 100. The testing value has also been checked to identify the model's effectiveness for unlearned data, as

shown in Figure 11, with detailed information in Table 4. All R^2 of the testing data show values of more than 0.8, demonstrating the machine learning capability for prediction.

3.2 The Predicted Magnetic Simulations and Pressure Drop

The predicted magnetic simulation values from the artificial neural networks are then compared with FEMM. Figure 12 compares the FEMM simulation results and DNN prediction at a given electrical current of 0.5 A. From Figure 12a, increasing the radial and annular gap can decrease the magnetic field at the annular zone because the magnetic flux needs to go through more resistance to complete one loop. Both simulation results give similar results. Several differences exist, but the machine learning method has still successfully captured the phenomena. The pattern seems different from that of the outer radial zone as the increase of the annular gap can increase the magnetic fields. It can be easily understood that the magnetic field must go through both outer annular and outer radial, as shown in Figure 2. Suppose the resistance in the outer annular increases, represented by the gap increase, while the radial gap is fixed. In that case, the magnetic field will gradually move to the outer radial part. In this phenomenon, the DNN can still predict the magnetic field with a similar pattern.

The capabilities of the DNN for capturing the effect of electrical current toward the predicted magnetic field densities are also observed. Figure 13 shows that, in general, DNN can replicate the pattern at various given electrical currents. The increase of the given electrical current can affect the magnetic field densities. Several parameters also affect the correlation, including dimension and the obstacle for performing a loop magnetic field. It is observed that the higher electrical current has a slight difference from the FEMM simulation results. The reason can be caused by the high nonlinearity for higher electrical current while predicting a high magnetic field density value.

The comparison is also conducted to check the visual representation along the observation lines, as shown in Figure 14. The annular and radial parts are the only pressure drops calculated, while the inner annular and orifices are ignored. The DNN predictions are slightly higher at inner radial gaps than the FEMMs. However, the visualization generally shows a good agreement between the DNN and FEMM magnetic flux lines.

The nonlinearity, proportional, and inverse proportional relation can also be identified using Pearson correlation among the variables. Table 5 reveals that electrical current exhibits the strongest positive correlation with both annular and outer radial magnetic field density, with correlation coefficients of 0.88 and 0.66, respectively. This strong positive relationship is expected, as increasing current typically enhances

the magnetic flux density within the valve. Conversely, radial gaps display a negative correlation with $B_{radial,outer}$ (-0.53) and a moderate negative correlation with $B_{annular}$ (-0.18). These negative correlations suggest that larger radial gaps may impede the magnetic flux, reducing the magnetic field density in these regions. Annular gaps show a negative correlation with $B_{annular}$ (-0.26). All gap sizes have a negative correlation with all predicted magnetic field densities, except magnetic field density at the outer radial $B_{radial,outer}$ as discussed and shown in Figure 13 previously.

The presence of nonlinear correlations is evident from the relatively low Pearson coefficients in some instances, such as the weak negative correlation between radial gaps and $B_{annular}$ (-0.18). These lower values suggest that the relationship between these variables may not be strictly linear, potentially due to complex geometric configurations or saturation effects within the magnetic material. As a result, relying solely on linear correlation may not fully capture the intricacies of these interactions, highlighting the importance of employing nonlinear modeling techniques like DNN to predict magnetic flux densities and subsequent pressure drops accurately.

The derived yield pressure drop based on the magnetic flux predicted by the DNN and FEMM values are also compared. The yield pressure drop is the pressure drop that is affected by magnetic field density, as shown in Eq. 6 and 9. When calculating the total pressure drop, the yield pressure drop will be combined with a viscous pressure drop affected by only the flow rate. Figure 15 compares the pressure drop yield between DNN and FEMM at various radial gap sizes at 1 A. The pressure drop from DNN is slightly higher than that of the FEMM-based pressure drop. The reason can be caused by the fact the training data is taken from the highest magnetic field at the zone. The pressure drops at 0.5 mm of annular and radial gaps also have similar results to the described peak pressure drop in the previous work [7]. The experimental and predicted DNN results have a difference of approximately 9.45%.

4 Conclusion

In conclusion, this study introduces a novel approach for predicting pressure drop in meandering MR valves using DNNs. The DNNs are trained to predict magnetic flux density, which is then utilized to forecast MR fluid yield stress and calculate pressure drop. The proposed models exhibit significant agreement with experimental results, highlighting the effectiveness of DNNs in capturing the intricate dynamics associated with pressure drop in meandering MR valves. The meandering flow path-type MR valve structure considered in this study involves complex geometries and various parameters, including annular and radial gaps, current, and channel lengths. The DNN models are carefully tuned using grid search cross-validation, exploring hyperparameters such as the number of hidden layers, the number of neurons in each layer, and activation functions. The results demonstrate that a three-layer DNN with ReLU activation in the first two

layers and Tanh activation in the third layer with 100 neurons yields optimal performance. The DNN models are validated through comparisons with finite element simulations using FEMM software. The predictions of magnetic flux density at different zones, including annular and outer radial, show good agreement with the referenced data.

Additionally, the DNN models successfully capture the impact of electrical current variations on magnetic field densities. The study also compares the yield pressure drop values predicted by DNNs with those obtained from FEMM simulations. While the DNN-predicted values are slightly higher, the overall agreement indicates the capability of DNNs to predict pressure drop in meandering MR valves. In summary, the application of DNN in predicting pressure drop in meandering MR valves proves to be a promising and effective approach. The developed models accurately capture complex relationships within the valve structure, making them valuable for optimizing and enhancing the performance of smart materials in engineering applications.

Future work will focus on expanding the range of design parameters to accommodate more complex valve geometries and diverse operational conditions. Integrating the surrogate DNN model with metaheuristic optimization algorithms will enable multi-objective valve design optimization. Further experimental validations across a broader spectrum of design parameters will enhance the model's accuracy and reliability.

Acknowledgment

This study is supported by Universitas Gadjah Mada Through Collaboration Research Program Southeast and South Asia And Taiwan Universities Joint Research Scheme (SATU JRS) 2023 with no 8778/UN1.P.II/Dit-Lit/PT.01.03/2023.

References

1. Tell, S., Andersson, A., Najafi, A., et al., “Real-time hybrid testing for efficiency assessment of magnetorheological dampers to mitigate train-induced vibrations in bridges”, *Int. J. Rail Transp.*, **00**(00), pp. 1–20 (2021). https://doi.org/10.1080/23248378.2021.1954560.

2. Zhang, Y., Guo, J., Yang, J., et al., “Recent Structural Developments and Applications of Magnetorheological Dampers (MRD): A Review”, *Magnetochemistry*, **9**(4), p. 90 (2023). https://doi.org/10.3390/magnetochemistry9040090.

3. Wu, Y., Zeng, J., Shi, H., et al., “A hybrid damping control strategy for high-speed trains running on existing tracks”, *J. Low Freq. Noise Vib. Act. Control*, **41**(3), pp. 1258–1271 (2022).

https://doi.org/10.1177/14613484221087513.

4. Liu, G., Gao, F., Wang, D., et al., "Medical applications of magnetorheological fluid: a systematic review", *Smart Mater. Struct.*, **31**(4), p. 043002 (2022). https://doi.org/10.1088/1361-665X/ac54e7.

5. Gołdasz, J., Sapiński, B., Kubík, M., et al., "Review: A Survey on Configurations and Performance of Flow-Mode MR Valves", *Appl. Sci.*, **12**(12) (2022). https://doi.org/10.3390/app12126260.

6. Abdalaziz, M., Vatandoost, H., Sedaghati, R., et al., "Development and experimental characterization of a large-capacity magnetorheological damper with annular-radial gap", *Smart Mater. Struct.*, **31**(11), p. 115021 (2022). https://doi.org/10.1088/1361-665X/ac9a16.

7. Imaduddin, F., Amri Mazlan, S., Azizi Abdul Rahman, et al., "A high performance magnetorheological valve with a meandering flow path", *Smart Mater. Struct.*, **23**(6), p. 065017 (2014). https://doi.org/10.1088/0964-1726/23/6/065017.

8. Zhu, J., Yang, X., Xie, G., et al., "Design and damping performance analysis of a multistage meandering hybrid valved magnetorheological damper", *Phys. Scr.*, **99**(4), p. 045517 (2024). https://doi.org/10.1088/1402-4896/ad31ed.

9. Idris, M. H., Imaduddin, F., Ubaidillah, et al., "A Concentric Design of a Bypass Magnetorheological Fluid Damper with a Serpentine Flux Valve", *Actuators*, **9**(1), p. 16 (2020). https://doi.org/10.3390/act9010016.

10. Hu, G., Qi, H., Zheng, K., et al., "Design and performance evaluation of a magnetorheological valve with mosquito-coil-plate fluid flow channels", *Sensors Actuators A Phys.*, **347**(November), p. 113983 (2022). https://doi.org/10.1016/j.sna.2022.113983.

11. Jiang, M., Rui, X., Yang, F., et al., "Multi-objective optimization design for a magnetorheological damper", *J. Intell. Mater. Syst. Struct.*, **33**(1), pp. 33–45 (2022). https://doi.org/10.1177/1045389X211006907.

12. Keshav, M., Bhagyarajan, A., and Chandramohan, S., "Regression models for magnetic flux density using DoE techniques and geometric optimization of MR valve", *Smart Mater. Struct.*, **28**(7), p. 075008 (2019). https://doi.org/10.1088/1361-665X/ab1e1b.

13. Olivier, M. and Sohn, J. W., "Design and geometric parameter optimization of hybrid magnetorheological fluid damper", *J. Mech. Sci. Technol.*, **34**(7), pp. 2953–2960 (2020).

https://doi.org/10.1007/s12206-020-0627-0.

14. Hu, G., Wu, L., Deng, Y., et al., "Optimal design and performance analysis of magnetorheological damper based on multiphysics coupling model", *J. Magn. Magn. Mater.*, **558**, p. 169527 (2022). https://doi.org/10.1016/j.jmmm.2022.169527.

15. Strecker, Z., Jeniš, F., Kubík, M., et al., "Novel approaches to the design of an ultra-fast magnetorheological valve for semi-active control", *Materials (Basel).*, **14**(10) (2021). https://doi.org/10.3390/ma14102500.

16. Yucesan, Y. A., Viana, F. A. C., Manin, L., et al., "Adjusting a torsional vibration damper model with physics-informed neural networks", *Mech. Syst. Signal Process.*, **154**, p. 107552 (2021). https://doi.org/10.1016/j.ymssp.2020.107552.

17. Luong, Q.-V., Jo, B.-H., Hwang, J.-H., et al., "A Supervised Neural Network Control for Magnetorheological Damper in an Aircraft Landing Gear", *Appl. Sci.*, **12**(1), p. 400 (2021). https://doi.org/10.3390/app12010400.

18. Saharuddin, K. D., Ariff, M. H. M., Mohmad, K., et al., "Prediction Model of Magnetorheological (MR) Fluid Damper Hysteresis Loop using Extreme Learning Machine Algorithm", *Open Eng.*, **11**(1), pp. 584–591 (2021). https://doi.org/10.1515/eng-2021-0053.

19. Wang, G., Qu, W., Chen, C., et al., "A road level identification method for all-terrain crane based on Support Vector Machine", *Measurement*, **187**, p. 110319 (2022). https://doi.org/10.1016/j.measurement.2021.110319.

20. Lv, H., Sun, Q., and Ma, W., "Data-driven prediction-control system modeling for magnetorheological damping force", *J. Intell. Mater. Syst. Struct.*, **34**(2), pp. 155–167 (2023). https://doi.org/10.1177/1045389X221103784.

21. Gupta, P., Pal, A., and Vittal, V., "Coordinated Wide-Area Damping Control Using Deep Neural Networks and Reinforcement Learning", *IEEE Trans. Power Syst.*, **37**(1), pp. 365–376 (2022). https://doi.org/10.1109/TPWRS.2021.3091940.

22. Lv, Y., Hui, J., Zhong, et al., "Online Learning Deep Neural Network Fuzzy Control of Structures Under Earthquake Motions: Numerical and Experimental Tests", *Int. J. Struct. Stab. Dyn.* (2024). https://doi.org/10.1142/S0219455425501433.

23. Duchanoy, C. A., Moreno-Armendáriz, M. A., Moreno-Torres, J. C., et al., "A deep neural network based model for a kind of magnetorheological dampers", *Sensors (Switzerland)*, **19**(6),

pp. 1–18 (2019). https://doi.org/10.3390/s19061333.

24. Hu, Y., Guo, W., Long, Y., et al., "Physics-informed deep neural networks for simulating S-shaped steel dampers", *Comput. Struct.*, **267** (2022). https://doi.org/10.1016/j.compstruc.2022.106798.

25. Imaduddin, F., Mazlan, S. A., Ubaidillah, et al., "Characterization and modeling of a new magnetorheological damper with meandering type valve using neuro-fuzzy", *J. King Saud Univ. - Sci.*, **29**(4), pp. 468–477 (2017). https://doi.org/10.1016/j.jksus.2017.08.012.

26. Saharuddin, K. D., Ariff, M. H. M., Bahiuddin, I., et al., "Non-parametric multiple inputs prediction model for magnetic field dependent complex modulus of magnetorheological elastomer", *Sci. Rep.*, **12**(1), p. 2657 (2022). https://doi.org/10.1038/s41598-022-06643-4.

27. Reyad, M., Sarhan, A. M., and Arafa, M., "A modified Adam algorithm for deep neural network optimization", *Neural Comput. Appl.*, **35**(23), pp. 17095–17112 (2023). https://doi.org/10.1007/s00521-023-08568-z.

28. Yang, X., Bi, F., Cheng, J., et al., "A Multiple Attention Convolutional Neural Networks for Diesel Engine Fault Diagnosis", *Sensors*, **24**(9) (2024). https://doi.org/10.3390/s24092708.

29. Bahiuddin, I., Imaduddin, F., Mazlan, S. A., et al., "Accurate and fast estimation for field-dependent nonlinear damping force of meandering valve-based magnetorheological damper using extreme learning machine method", *Sensors Actuators A Phys.*, **318**, p. 112479 (2021). https://doi.org/10.1016/j.sna.2020.112479.

30. Vu, H. L., Ng, K. T. W., Richter, A., et al., "Analysis of input set characteristics and variances on k-fold cross validation for a Recurrent Neural Network model on waste disposal rate estimation", *J. Environ. Manage.*, **311**, p. 114869 (2022). https://doi.org/10.1016/j.jenvman.2022.114869.

31. Carmona, I. C., Kumbhare, D., Baron, M. S., et al., "Quintuple AISI 1010 carbon steel core coil for highly focused transcranial magnetic stimulation in small animals", *AIP Adv.*, **11**(2), pp. 1–8 (2021). https://doi.org/10.1063/9.0000219.

32. Nguyen, Q. H., Choi, S. B., and Wereley, N. M., "Optimal design of magnetorheological valves via a finite element method considering control energy and a time constant", *Smart Mater. Struct.*, **17**(2) (2008). https://doi.org/10.1088/0964-1726/17/2/025024.

List of Figures

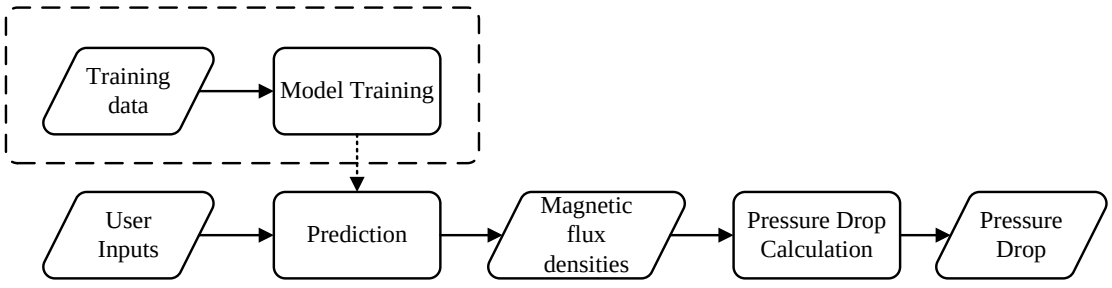

Figure 1. The proposed systematic procedure to predict pressure drops

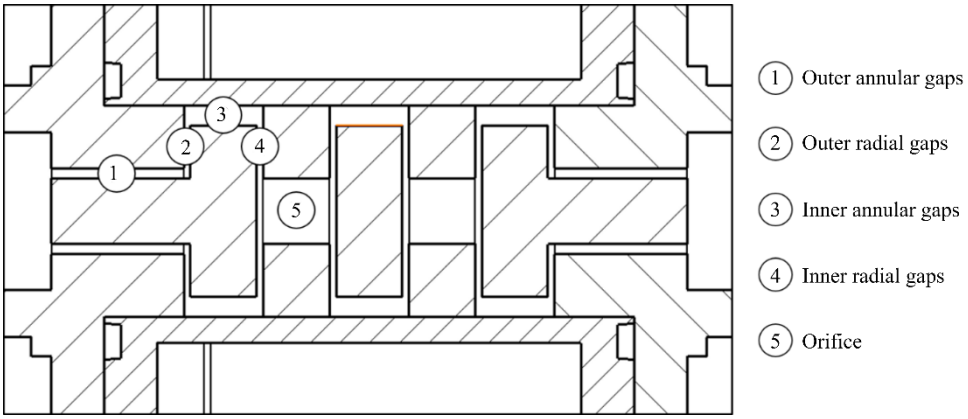

Figure 2. Meandering Flow Path

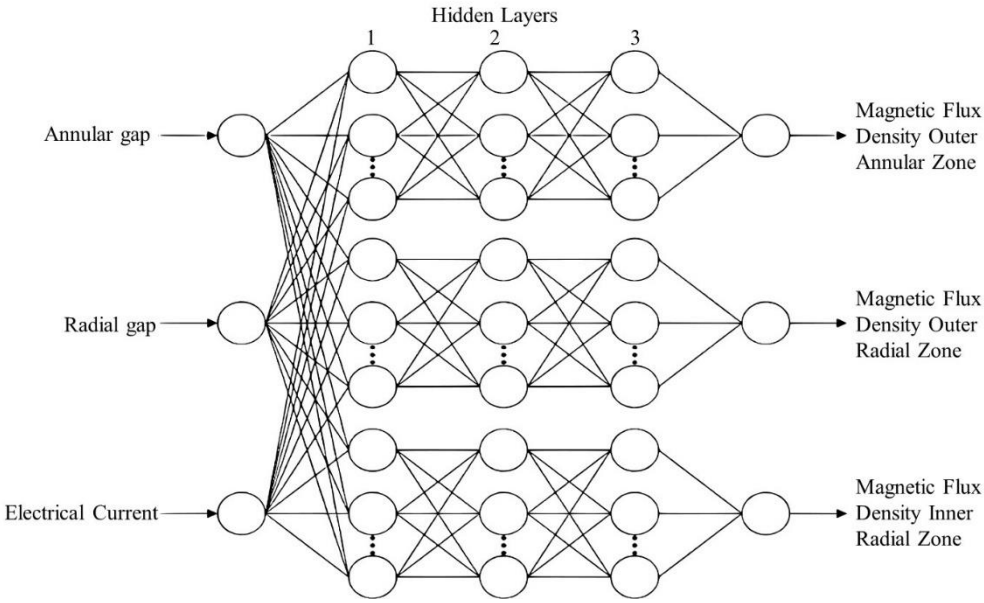

Figure 3. The proposed DNN architectures

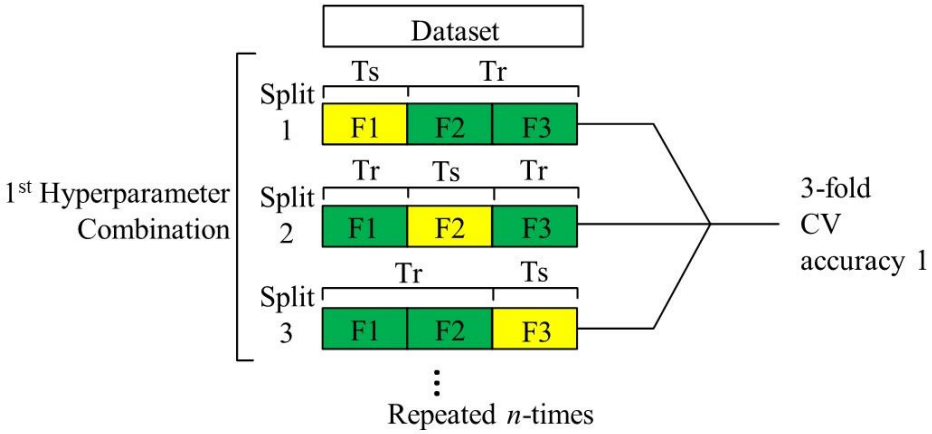

Figure 4. Grid Search Cross-Validation Process

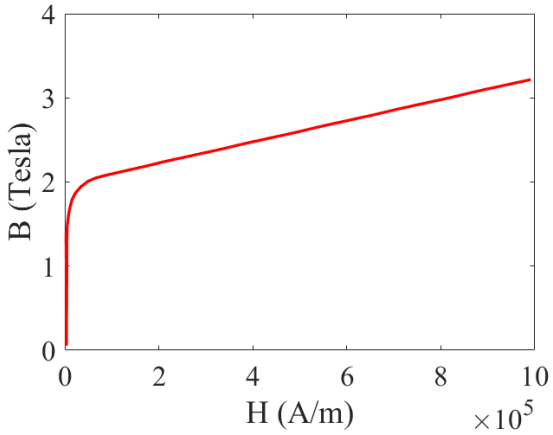

Figure 5. AISI 1010 Carbon steel BH Curve [31]

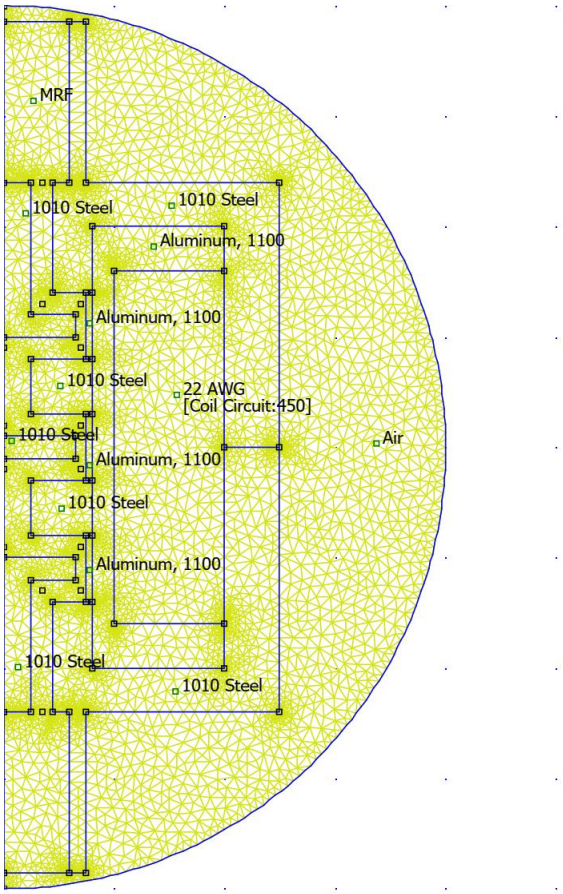

Figure 6. 2D axisymmetric Design of MR valve with meandering flow path type in FEMM Software

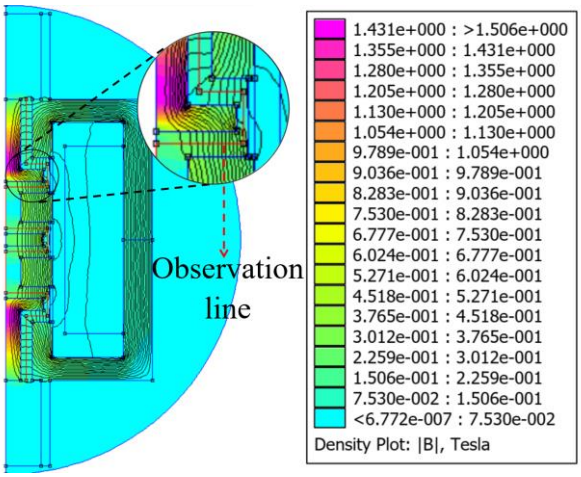

Figure 7. The observation line for measuring the magnetic flux densities

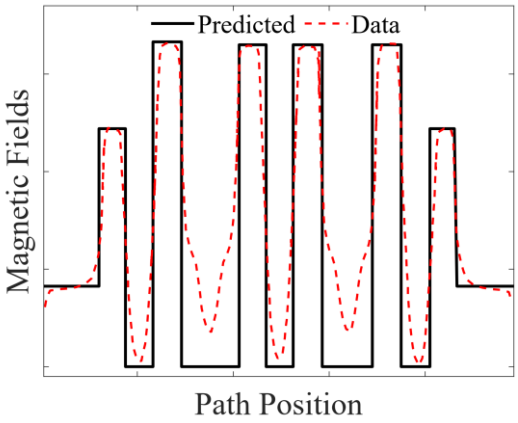

Figure 8. Illustration of the training data determination

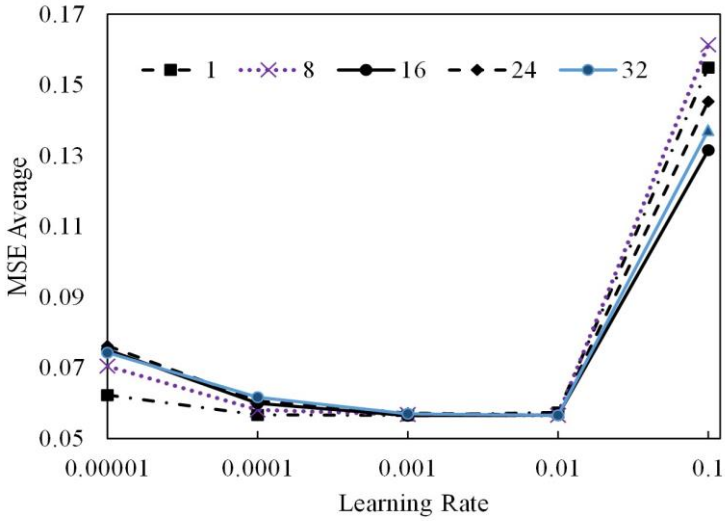

Figure 9. MSE at various learning rates and batch sizes

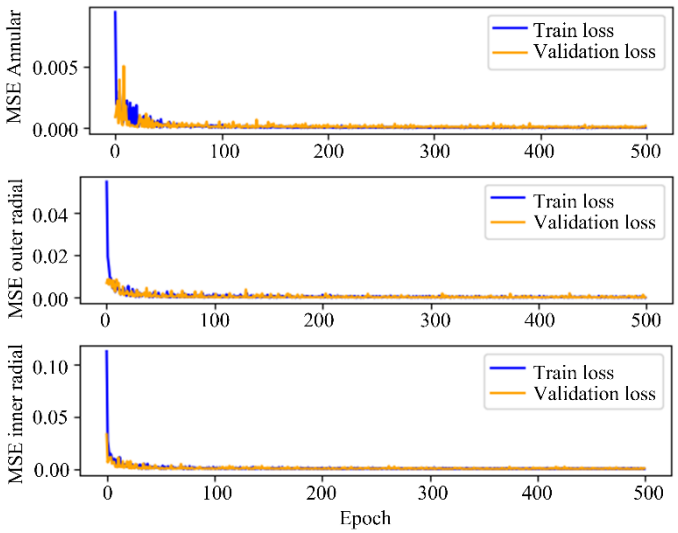

Figure 10. MSE over epochs at various zones for the training process

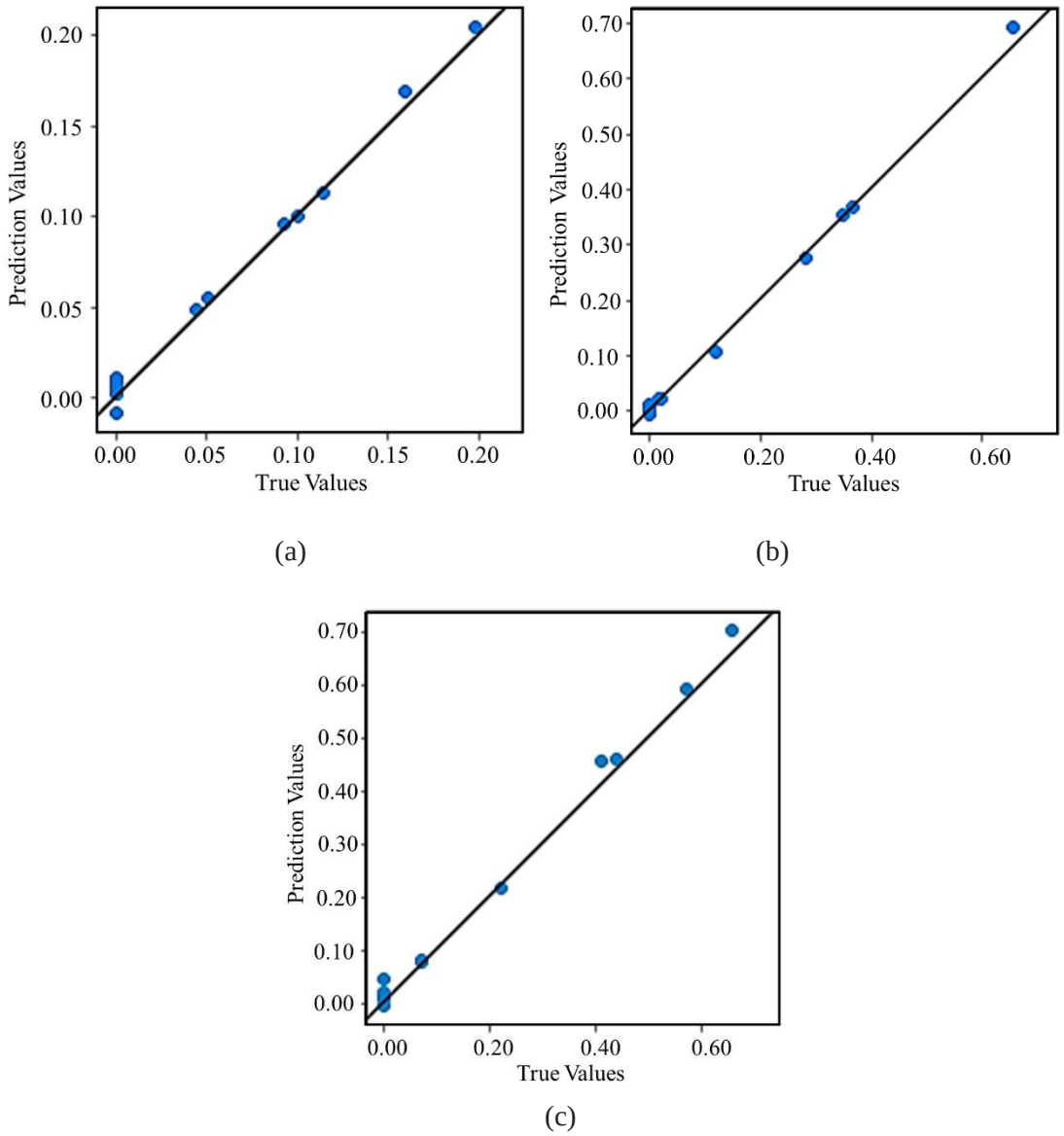

Figure 11. Testing regression plot at (a) annular zone, (b) outer radial zone, (c) inner radial zone

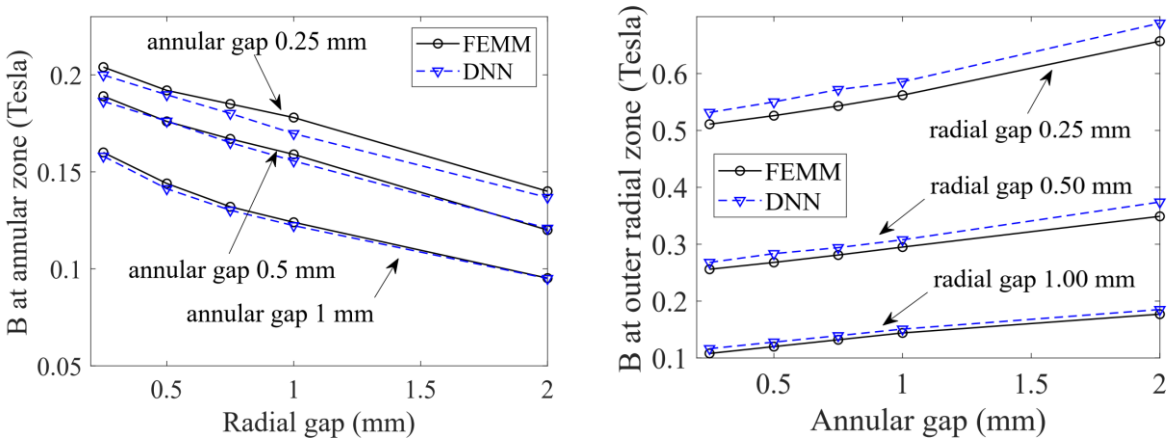

(a) (b)

Figure 12. Magnetic flux density at annular zone (a) and outer radial zone (b) as a function of various gap dimensions

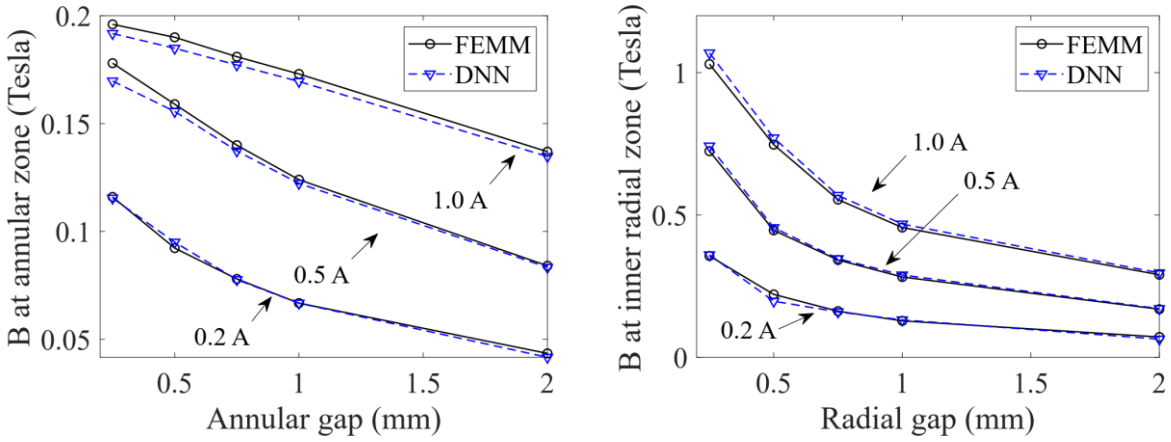

(a) (b)

Figure 13. Magnetic flux density at annular zone (a) and inner radial zone (b) as a function of the given electrical currents

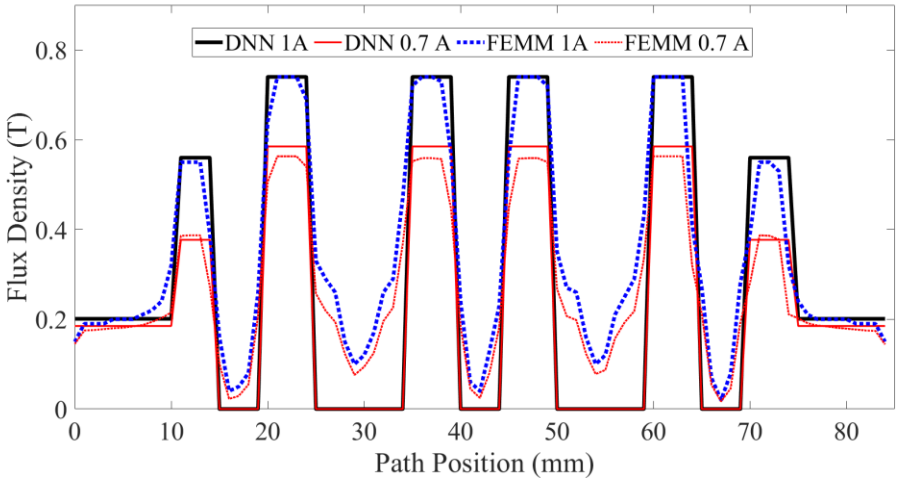

Figure 14. Magnetic flux densities comparison along the observation line

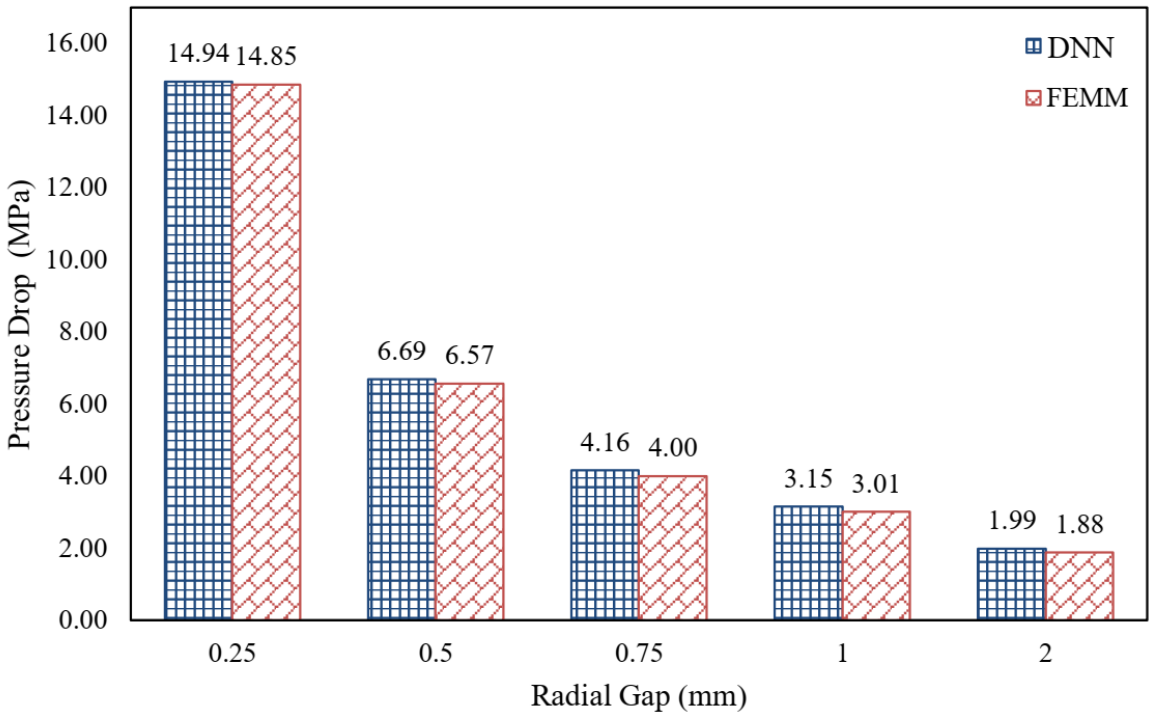

Figure 15. Comparison of yield pressure drop values between DNN and FEMM simulations

List of Tables

Table 1. DNN Hyperparameters

Hyperparameters	**Values**
Hidden layer Number	1-3 layer
Hidden Neuron Number	10 - 100
Activation Functions	ReLU, sigmoid, tanh
Learning Rate	10^{-1} - 10^{-5}
Batch size	11,689

Table 2. MR valve parameters

Parameters	Descriptions	Value	Units
η (MRF-132DG)	Fluid viscocity	0.112	Pa s
Q	Flow rate	40	ml/s
d_{ao}	Outer annular gap size	0.5 - 2	mm
$d_r = d_{ro} = d_{ri}$	Radial gap size	0.5 - 2	mm
d_{ai}	Inner annular gap size	1	mm
L_{ao}	Outer annular channel length	10	mm
L_{ai}	Inner annular channel length	6 - $2d_r$	mm
L_o	Orifice channel length	5	mm
R_1	Outer radius of radial gap	6.5	mm
R_{0_outer}	Inner radius of the outer radial gap	2.5 + d_{ao}	mm
R_{0_inner}	Inner radius of the inner radial gap	2.5	mm

Table 3. MSE training at various hidden node numbers

Activation Function			MSE at Hidden Number of		
First Layer	Second Layer	Third Layer	10	50	100
Sig	-	-	0.17	0.14	0.12
Tanh	-	-	0.1	0.08	0.08
ReLU	-	-	0.12	0.08	0.07
Sig	Sig	-	0.16	0.16	0.16
Sig	Tanh	-	0.17	0.12	0.14
Sig	ReLU	-	0.14	0.13	0.11
Tanh	Sig	-	0.13	0.08	0.08
Tanh	Tanh	-	0.09	0.08	0.08
Tanh	ReLU	-	0.09	0.07	0.07
ReLU	Sig	-	0.25	0.08	0.07
ReLU	Tanh	-	0.11	0.07	0.07
ReLU	ReLU	-	0.09	0.07	0.07
Sig	Sig	Sig	0.35	0.17	0.17
Tanh	Tanh	ReLU	0.08	0.07	0.06
Tanh	ReLU	Sig	0.11	0.07	0.06
Tanh	ReLU	Tanh	0.08	0.07	0.06
Tanh	ReLU	ReLU	0.08	0.06	0.06
ReLU	Sig	Sig	0.26	0.08	0.1
ReLU	Tanh	Sig	0.14	0.07	0.07
ReLU	Tanh	Tanh	0.09	0.07	0.07
ReLU	Tanh	ReLU	0.08	0.06	0.06
ReLU	ReLU	Sig	0.12	0.07	0.06
ReLU	ReLU	Tanh	0.08	0.07	0.06
ReLU	ReLU	ReLU	0.08	0.07	0.06

Table 4. R^2 training and testing at selecting schemes

Activation Functions			R^2 Training			R^2 Test		
1st Layer	2nd Layer	3rd layer	Output 1	Output 2	Output 3	Output 1	Output 2	Output 3
Relu	ReLU	ReLU	0.99	1.00	1.00	0.99	0.99	1.00
ReLU	ReLU	Tanh	0.99	1.00	1.00	0.99	0.98	0.99
Sigmoid	Tanh	ReLU	0.98	1.00	1.00	0.99	0.98	1.00
ReLU	Sigmoid	ReLU	0.89	1.00	1.00	0.96	0.90	0.99

Table 5. Correlation among variables

	Annular Gap	Radial Gap	Current	$B_{annular}$	$B_{radial,outer}$	$B_{radial,inner}$
Annular Gap	1	0	0	-0.26	0.08	-0.03
Radial Gap	0	1	0	-0.18	-0.53	-0.47
Current	0	0	1	0.88	0.66	0.77
$B_{annular}$	-0.26	-0.18	0.88	1	0.69	0.83
$B_{radial,outer}$	0.08	-0.53	0.66	0.69	1	0.97
$B_{radial,inner}$	-0.03	-0.47	0.77	0.83	0.97	1

Biography

Hafizh Arsa Prabhakara received his degree in Heavy Equipment Maintenance and Management Technology from Universitas Gadjah Mada (UGM) in 2021. His research focuses on machine learning applications in magnetorheological (MR) devices, forklift hydraulics, and dynamic modeling. He has developed machine learning model for smart actuator, bond graph models for analyzing hydraulic leakage in forklift lifting mechanisms, and artificial neural networks for modeling the damping force of meandering MR dampers. His work integrates computational simulations, optimization techniques, and experimental validation to improve the design, control, and performance of MR systems and heavy equipment.

Fitrian Imaduddin received his Sarjana Teknik degree (Equivalent with Bachelor degree in Engineering) in Engineering Physics from ITS, Indonesia; M.Sc degree in Mechanical Engineering from UTeM, Malaysia; and Ph.D. in Magnetorheological (MR) Actuator from Universiti Teknologi Malaysia (UTM). His current research interest is related with modeling and control of dynamic systems especially the ones involving smart materials and actua- tors. He is currently a faculty member of the Mechanical Engineering Program, Faculty of Engineering, Universitas Sebelas Maret, Indonesia.

Azizan Bin As'arry received his B.Eng. in Mechanical Engineering from Universiti Teknologi Malaysia (UTM) in 2008, followed by an M.Eng. in Mechanical Engineering (Control) from UTM in 2009. He then obtained his Ph.D. in Mechanical Engineering (Control) from UTM in 2014, with a research focus on Intelligent Active Force Control of Human Hand Tremor using Smart Actuator. His research interests include active force control, vibration and tremor control, intelligent optimization techniques such as Genetic Algorithm and Particle Swarm Optimization, and system identification. He is currently a Senior Lecturer in the Department of Mechanical and Manufacturing Engineering, Faculty of Engineering, Universiti Putra Malaysia (UPM).

Andhi Akhmad Ismail received his S.T. degree in Mechanical Engineering from Institut Teknologi Bandung (ITB) in 2002. He then earned his M.Eng. degree in Electrical Engineering from Universitas Gadjah Mada (UGM) in 2012, focusing on the application of the Ant System algorithm for optimizing routes in the Traveling Salesman Problem (TSP) with road condition constraints. His research interests include automation and instrumentation. He is currently a lecturer in the Department of Mechanical Engineering, Vocational College, Universitas Gadjah Mada (UGM).

Professor Saiful Amri Mazlan is a registered Professional Engineer with Board of Engineers Malaysia. He holds a Doctorate degree from Dublin City University, Ireland. He is currently a Professor at MJIIT-UTM. His research is primarily in the area of magnetorheological (MR) fluids, where this material undergoes significant responses lead- ing to consequent rheological changes upon the influence of an

external field. The same phenomenon also hap- pens to MR elastomer, where both materials can offer tremendous opportunities for variable stiffness devices. He managed to publish his research works in several inter- national journals and conference proceedings

Irfan Bahiuddin is a senior lecturer at Department of Mechanical Engineering, Vocational College, Universitas Gadjah Mada (UGM), Indonesia. He earned his degree from Institut Teknologi Bandung (ITB), Indonesia, in 2012. He received his master and Ph.D. from Malaysia-Japan International Institute of Technology (MJIIT), Universiti Teknologi Malaysia (UTM) in 2016 and 2019, respectively. His research focusses on the machine learning, bond graph, dynamic model simulation, optimization method, and magnetorheological material/device rheological properties evaluation. He has also worked in other research areas, such as turbocharger, railway vehicle, and vibration monitoring.